# Improved Suppression of Beam-Tunnel Parasitic Oscillations by Introducing Lossy Diffusive Surfaces

Athanasios I. Zelkas, George P. Latsas, Dimitrios V. Peponis, Konstantinos A. Avramidis, and Ioannis G. Tigelis, *Senior Member, IEEE*

***Abstract*— High-power gyrotrons usually suffer from parasitic oscillations, appearing in the beam tunnel region, which degrade the electron beam quality and the interaction efficiency in the cavity. To avoid the development of such oscillations, several design concepts have been proposed and tested in the past, including the stacked beam tunnel concept, the ceramic-loaded smooth-wall beam tunnel, and the fully metallic beam tunnel with broken symmetry. In this work, we focus on the fully metallic concept by examining the possibility of using diffusive surfaces to effectively suppress the parasitic modes. To this end, a beam tunnel with a diffusive surface is designed, having dimensions that are compatible with a typical high-power gyrotron. The performance of the structure is studied by full-wave particle-in-cell (PIC) beam-wave interaction simulations and is compared to that of a smooth metallic beam tunnel of the same dimensions. Both low- and high-Ohmic wall losses are considered in the study. Simulation results demonstrate that the diffusive surface can indeed secure an almost perfect suppression of the parasitic modes, even when the Ohmic wall losses are quite low, i.e., similar to those of copper.**

***Index Terms*— Beam tunnel, fully metallic, gyrotron, parasitic oscillations.**

## I. Introduction

GYROTRONS are high-frequency, high-power millimeter-wave sources, commonly used for electron cyclotron resonance heating (ECRH) and current drive in magnetic confinement fusion reactors [1], [2], [3]. The beam tunnel is a critical component of a high-power gyrotron, since it serves as the drifting region where the electron beam undergoes compression under the influence of an axially varying magnetostatic field, acquiring the necessary characteristics for the main interaction in the main interaction cavity [3], [4], [5]. However, the premature beam-wave interaction, which may appear in this region leading to the development of parasitic oscillations, has always been a persistent challenge [6], [7], [8], [9], [10], [11]. Such oscillations impact the quality of the electron beam and subsequently reducing the efficiency of the primary interaction within the cavity.

In response to this challenge, various design strategies have been implemented to optimize the beam tunnel performance by suppressing the parasitic oscillations, often leading to quite complicated and sophisticated structures [7], [8], [9], [10], [11], [12], [13]. They often adopt configurations such as stacked sequences of metallic and lossy ceramic rings, a concept mainly implemented in European gyrotrons [12], [14], or tapered waveguides loaded with lossy silicon carbide (SiC), mostly used in Japanese gyrotrons [10]. Fully metallic beam tunnels with arbitrary surface corrugations are a concept mainly used in Russian gyrotrons [1], [11]. Notably, the latter concept has garnered attention for the simplicity in design and fabrication procedures [15].

With respect to beam-tunnel concepts involving ceramic materials, previous studies have shown that, while azimuthal corrugations at the metallic rings of stacked beam tunnels may impact parasitic oscillations [7], the dielectric properties significantly influence the beam tunnel's ability to suppress them [8], [9], [13]. On the other hand, smooth-wall SiC-loaded beam tunnels have performed well [16]. Many studies have investigated the influence of geometric characteristics on parasitic oscillations offering alternative methods for their suppression through geometry and the selection of ceramic materials [8]–[19].

With the increasing demand for output power, the ability to operate at higher beam currents while suppressing spurious oscillations in the beam-tunnel area becomes even more challenging. Moreover, the move toward series production of gyrotrons necessitates beam-tunnel designs that are easier to manufacture, avoiding the use of costly and complex dielectric materials. In this direction, the European 1 MW, 170 GHz short-pulse modular gyrotron was tested experimentally with a fully metallic beam tunnel, offering promising results. Operating currents close to 70 A enable the excitation of the nominal $TE_{32,9}$ mode at a power above 1.2 MW, without detecting any parasitic oscillations [20].

Manuscript received 15 May 2024; revised 17 June 2024; accepted 19 June 2024. Date of publication 1 July 2024; date of current version 25 July 2024. This work has been carried out within the framework of the EUROfusion Consortium, funded by the European Union via the Euratom Research and Training Programme (Grant Agreement No 101052200—EUROfusion). Views and opinions expressed are however those of the author(s) only and do not necessarily reflect those of the European Union or the European Commission. Neither the European Union nor the European Commission can be held responsible for them. The publication of the article in OA mode was financially supported by HEAL-Link. The review of this article was arranged by Editor D. Simon. *(Corresponding author: Athanasios I. Zelkas.)*

The authors are with the Department of Physics, National and Kapodistrian University of Athens, Zografou, 15784 Athens, Greece (e-mail: thazelkas@phys.uoa.gr).

Color versions of one or more figures in this article are available at https://doi.org/10.1109/TED.2024.3418299.

Digital Object Identifier 10.1109/TED.2024.3418299

Another approach, which has recently been proposed, involves the use of diffusive geometries on the inner metallic surfaces of a stacked beam tunnel, to achieve the effective diffusion and suppression of any excited parasitic oscillations [21], [22]. Schroeder diffusers, also known as quadratic residue diffusers (QRDs), are devices for the manipulation of acoustic waves, used to achieve uniform scattering of sound energy, contributing to enhanced acoustic performance [23], [24]. The simplicity of their design has made them among some of the most effective diffuser designs. In such a diffuser, sound waves incident to their surface are presumed to propagate vertically within each well, undergoing a phase shift, depending on the depth of the well. The organized phase modulation caused by the different wells leads to an almost uniform radiation pattern [25], [26], [27], [28]. Even though Schroeder diffusers have been extensively used in the field of acoustic waves, the same underlying principle of operation can well be adopted to electromagnetic structures [29], [30].

In this work, we study the possibility of using a diffusive geometry on the wall of a fully metallic beam tunnel to effectively suppress parasitic oscillations, by simulating corresponding structures in the CST Studio Suite [31]. This program offers the possibility of full-wave particle-in-cell (PIC) modeling. Therefore, the study of the actual interaction of the electron beam with parasitic RF waves in the beam tunnel is possible, in contrast to the studies in [21] and [22], which are addressing only the influence of the diffusive surface on the RF field structure and they are not considering the beam-wave interaction.

For our investigations, a smooth metallic tapered beam tunnel is initially considered, resembling the inner contour of the geometry of the existing TH1509v4 stacked beam tunnel of the 170 GHz 1 MW European gyrotron for ITER [20]. Self-consistent numerical simulations using the PIC solver of the CST Studio Suite are performed. The excited parasitic mode is identified and studied, through post-processing of the obtained fields. Next, Ohmic losses are gradually applied to the walls to study their effect on the parasitic modes. Then, a diffusive geometry is designed, based on the Schroeder diffuser theory, and added on the metallic walls of the model, both with and without losses, to evaluate the performance of the structure.

The rest of the article is organized as follows. In Section II, the smooth fully metallic model is presented along with the obtained results with and without losses. In Section III, the design procedure and simulation results for the beam tunnel model with diffusive surface are described, and in Section IV, the obtained results are compared and discussed. Finally, in Section V, the main conclusions are summarized.

## II. Smooth Fully Metallic Beam-Tunnel Model

We start with a smooth-wall fully metallic beam-tunnel model design, which will be used as the baseline beam-tunnel for this study. To secure relevance with a high-power gyrotron beam tunnel, this model design closely matches the dimensions of the beam tunnel of the 1 MW, 170 GHz European gyrotron for ITER [20]. In particular, the outer wall of the model was taken to closely follow the inner radius of the metallic walls of that stacked beam tunnel. At both ends, a narrow ring of constant radius was added, to facilitate the application of the boundary conditions. The right end of the model ($z = 0$) corresponds to the physical end of the beam tunnel (start of the spacer component between the beam tunnel and the cavity). The material of the outer wall of the model is the so-called perfect electric conductor (PEC) in CST, which represents an ideal lossless metal. The geometrical characteristics of the model are given in Table I and Fig. 1.

TABLE I
GEOMETRICAL PROPERTIES OF THE SMOOTH BEAM-TUNNEL MODEL

| $L_1$ (mm) | $L_2$ (mm) | $L_3$ (mm) | $L_{tot}=L_1+L_2+L_3$ (mm) | $a_1$ (mm) | $a_2$ (mm) |
|---|---|---|---|---|---|
| 2 | 67.8 | 2 | 71.8 | 14 | 18.5 |

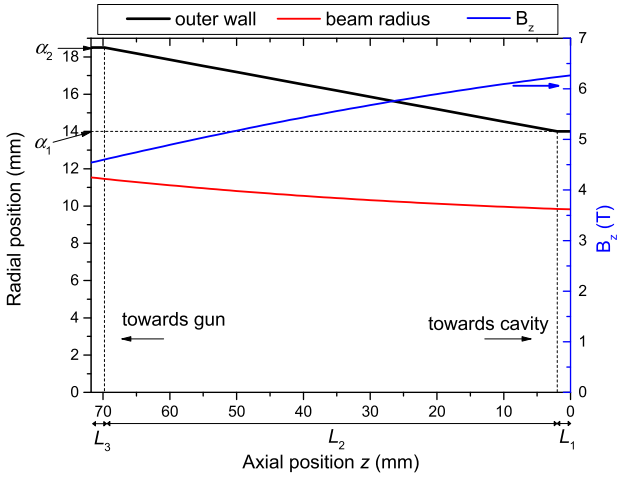


Fig. 1. Outer wall contour, the beam radius, and the magnetic field profile ($B_z$) of the smooth metallic beam-tunnel model. The geometrical properties of Table I are also shown.

A realistic, axially varying magnetostatic field was imposed with its profile given in Fig. 1. The electron beam was modeled as a ring-shaped emitting surface located at the beginning of the beam tunnel with initial parameters calculated by the adiabatic approximation, using their nominal values at the center of the cavity ($\gamma_{\text{nom}} = 1.156$, $\alpha_{\text{nom}} = 1.3$, $r_{b,\text{nom}} = 9.44$ mm). The exact values used are given in Table II. Spread has been defined in the relativistic factor $\gamma$ and the pitch angle $\alpha$ (Table II), both of which follow uniform distributions. A 3-D field monitor and a 3-D particle monitor were defined, along with several electric field probes to obtain the temporal and spatial field distributions and the evolution of the electron beam properties. Waveguide ports were defined at both ends of the structure, effectively absorbing any incident modes, thus minimizing the reflections. Note that waveguide ports are located at the last part of the structure and act as boundary conditions solely on the electromagnetic fields. Regarding the particles, the boundary at the end of the structure (after the ports) is defined as grounded PEC, absorbing any incident electrons without charging the boundary. A hexahedral mesh was used in the model, and several mesh density values were tested. It was found that with a mesh density of 12 cells per wavelength, adequate convergence was achieved. This mesh density was used in all simulations appearing in this work. The

TABLE II
INITIAL ELECTRON BEAM PARAMETERS

| $r_b$ (mm) | $\gamma_0$ | $\alpha = v_\perp/v_\parallel$ | $I_b$ (A) | $\gamma$ spread (% uniform) | $\alpha$ spread (% uniform) |
|---|---|---|---|---|---|
| 11.53 | 1.156 | 0.85 | 40 | 0.2% | 7% |

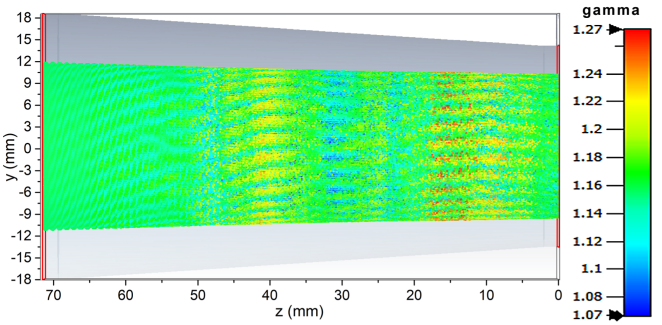


Fig. 2. Beam electrons position at 20 ns inside the 3-D structure, colored according to their gamma value. Axes have been manually added to enhance the readability of the figure.

simulations were performed in a 2-cpu, 20-core Intel Xeon machine and each simulation required from 10 to 60 days to finish, which is a consequence of the complexity of the structure, the appropriate mesh density, and the consideration of the losses. The total number of electrons inside the structure was of the order of $10^6$.

Fig. 2 shows the obtained electron position and $\gamma$ distribution (denoting their energy) at 20 ns, a timestep at which the excited fields have been adequately stabilized. In particular, it illustrates the electron positions inside the 3-D structure (shown in gray) colored according to their gamma value. From the color distribution of the electrons, energy modulation can be clearly seen, evidence of the development of oscillations. Fig. 3 presents the developed electric field distribution both in $r$-$z$ and $r$-$\varphi$ planes at the same timestep. From Fig. 3(a), it is evident that the developed fields clearly resemble the distribution of a propagating mode, with a maximum at around $z = 40$ mm. The transverse distribution at that axial location [Fig. 3(b)] resembles the field of an almost pure $TE_{27,5}$ mode. A slight asymmetry observed in the field distribution could be attributed to the superposition of the developed mode with either other excited modes with significantly smaller amplitude, or a possible reflection of the excited mode somewhere in the structure.

Fig. 4 shows the evolution of the total energy inside the structure with time (blue line), revealing that the simulation has converged after 17 ns without any sign of instability. In the same figure, the electric signal in the proximity of the field maximum ($r = 12$ mm, $z = 40$ mm) is also shown (black line). From this curve, it is also evident that after 17 ns the amplitude of the signal is almost constant, showing that steady state has been achieved.

To ascertain the excited frequency, a fast Fourier transform (FFT) was performed on the last part of the electric signal at $r = 12$ mm, $z = 40$ mm (Fig. 4), yielding the spectrum depicted in Fig. 5. An acute peak at 139.8 GHz can be clearly seen. Based on this frequency value, and in conjunction with

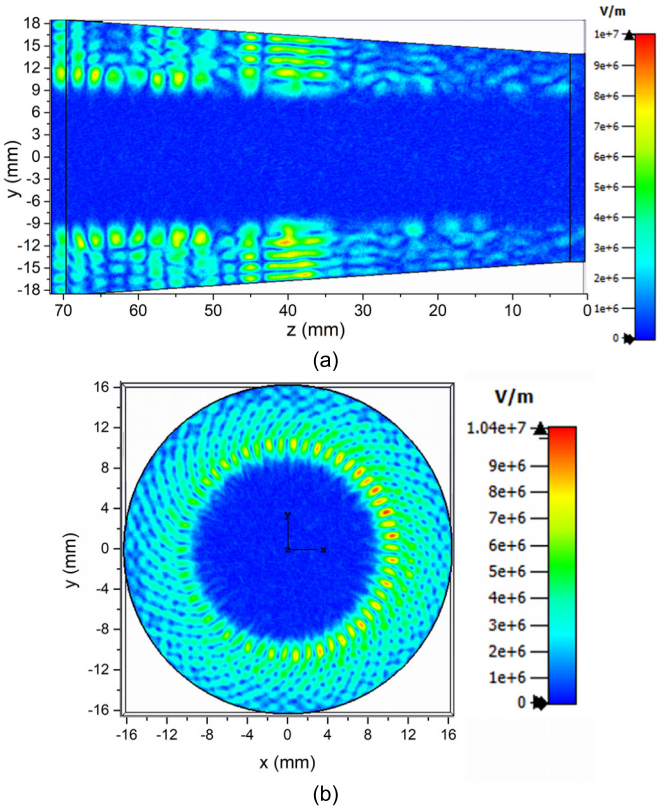


Fig. 3. Electric field magnitude distribution at 20 ns on (a) $yz$ plane and (b) cross section ($xy$ plane) at $z = 40$ mm.

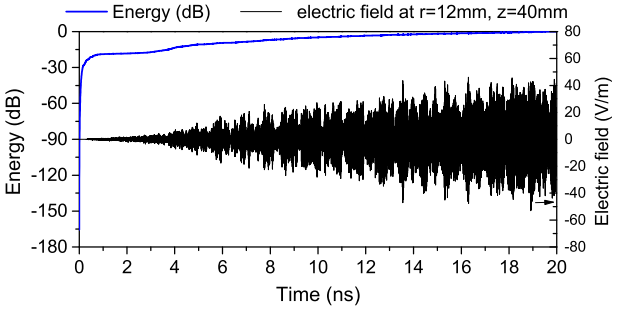


Fig. 4. Time evolution of the total energy inside the structure in dB (blue) and electric signal at ($r = 12$ mm, $z = 40$ mm) (black).

the zero-order approximation dispersion graph at $z = 40$ mm (Fig. 6), it can be deduced that the mode is a forward wave, excited at a position around $z = 40$ mm, which falls below cutoff and is totally reflected at a position around $z = 37$ mm. This observation is in good agreement with the obtained field distribution.

To study the effect of the finite conductivity of the metallic wall on the excited parasitic mode, losses were added and gradually increased. Fig. 7 shows the obtained power spectrum for the smooth lossless case (black line) and the smooth lossy case of copper at room temperature ($\sigma = 5.8 \times 10^7$ S/m) (blue line) as mean square amplitude (MSA). From this figure, only a small reduction of the peak value is observed, with the mode still excited. To achieve full suppression of the parasitic mode, a conductivity value as low as $\sigma = 10^5$ S/m with a roughness of 0.1 mm rms was required (Fig. 7, red line).

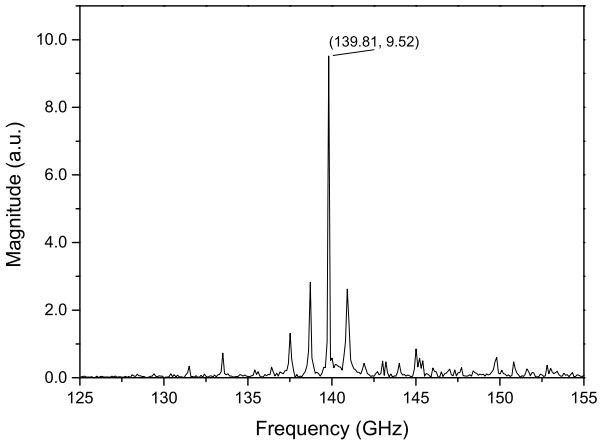


Fig. 5. Frequency spectrum of the electric signal at $r = 12$ mm and $z = 40$ mm for the smooth lossless model.

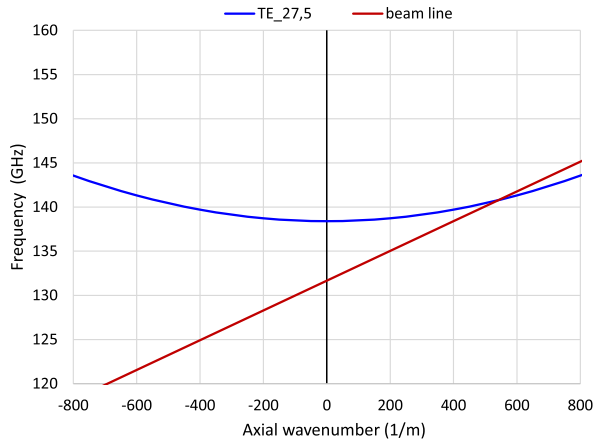


Fig. 6. Dispersion curve of the $TE_{27,5}$ mode and the beam line at $z = 40$ mm.

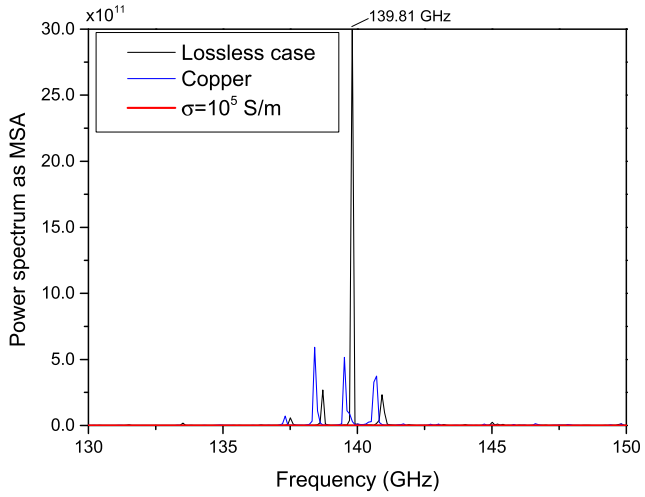


Fig. 7. Power spectrum of the electric field signal at $r = 12$ mm, $z = 40$ mm without losses (black line), for copper ($\sigma = 5.8 \times 10^7$ S/m) (blue line), and for $\sigma = 10^5$ S/m (red line), for the smooth model.

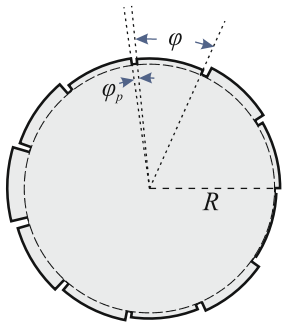


Fig. 8. Cross section of a diffusive geometry with $N = 11$, chosen here for illustrative purposes. All dimensions are indicative.

However, achieving such a low conductivity value with a metal alloy is quite challenging. This implies that coating the walls with some lossy material would be necessary for the concept of smooth metallic beam tunnels.

## III. Fully Metallic Model With Diffusive Surface

Even though Schroeder diffusers have been extensively used in the field of acoustic waves, the same underlying principle of operation can well be applied to electromagnetic structures. Therefore, the concept of using a diffusive geometry on the metallic walls for the suppression of parasitic modes in the beam tunnel was examined. The concept is based on the fact that the incident waves on such a geometry are diffused in a large range of angles and the development of standing waves is minimized. In a waveguide, this is equivalent to the diffusion of the power of a specific mode to a large number of other modes.

To add such a diffusive geometry on the walls of the smooth metallic beam tunnel, we chose to design a 1-D diffuser, applied on the azimuthal direction, while, axially, the wells have constant depth and azimuthal width along the $z$-axis and a total length equal to that of the beam tunnel. The geometry consists of $N$ wedge-shaped slots each with azimuthal width $\varphi = R^{-1}\lambda_{\min}/2$, where $R$ the inner radius of the walls and $\lambda_{\min}$ the minimum wavelength before cross-modes of the wells appear [26]. This means that the field with zero-order resonance will appear inside the slots only at that limiting wavelength. For wavelengths smaller than $\lambda_{\min}$, the diffuser will also work, but its performance will be reduced, achieving less uniform diffusion. Fig. 8 shows the cross section of such a geometry, in which $N = 11$ was assumed for illustrative purposes. The azimuthal width of the separating panels between the slots $\varphi_p$ was chosen to be small enough with respect to the wavelength to minimize any interaction between the panels and the waves. To achieve this, a value close to $\varphi_p = R^{-1}\lambda_{\min}/10$ would suffice [28]. The value $N$ should be a prime number and $N(\varphi + \varphi_p)$ should be equal to 360°. Thus, $N$ is chosen to closely satisfy this requirement and then $\varphi_p$ is determined by $\varphi_p = 360°/N - \varphi$. The depth of the $n$th slot ($n = 1, 2, \ldots, N$) is given by

$$d_n = \frac{S_n \lambda_0}{2N}$$

where $\lambda_0$ is the wavelength which corresponds to the design frequency and the quantity $S_n = n^2 \bmod N$, with mod denoting the integer modulo operation.

Since in our case the geometry is axially tapered, we had to choose a specific radius $R$ at a specific axial position to apply the aforementioned design principles. This position was

TABLE III
GEOMETRICAL CHARACTERISTICS OF THE DIFFUSER

| $\varphi$ (degrees) | $\varphi_p$ (degrees) | $N$ | $f_0$ (GHz) |
|---|---|---|---|
| 3.58 | 0.76 | 83 | 140 |

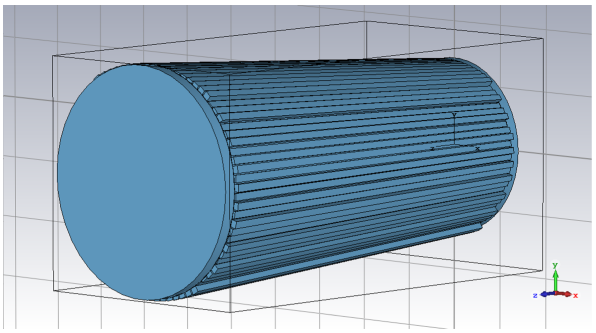

Fig. 9. Model of the beam-tunnel with Schroeder diffuser.

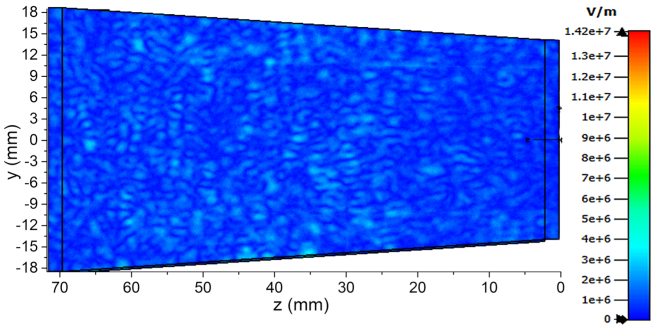


Fig. 10. Electric field magnitude distribution at 20 ns on the $r$-$z$ plane for the lossless diffuser model.

chosen to approximately match the axial position where mode excitation was observed in the smooth model case, i.e., $R = 16$ mm, $z = 40$ mm. The design frequency was selected close to the excited one, namely 140 GHz. The maximum frequency appearing in the relations above was chosen to be 150 GHz to include any possible modes with larger frequency. The final values are given in Table III. The developed model is shown in Fig. 9.

To allow direct comparison with the previously presented results, all the other simulation parameters were kept unmodified. Fig. 10 depicts the electric field distribution $|\mathbf{E}|$ on the $r$-$z$ plane at $t = 20$ ns. It is clear that the field distribution does not correspond to a single waveguide mode; it resembles a superposition of a large number of modes, with the field values being significantly reduced. The obtained electron energy distribution presents much smaller variations with no visible velocity modulation and bunching.

The power spectrum of the electric signal at $r = 12$ mm, $z = 40$ mm is presented in Fig. 11 (blue line). In the same figure, the corresponding distribution of the lossless smooth case is also depicted for comparison. It can be seen that in the case of the diffusive geometry, the amplitude of the peaks was significantly reduced, corresponding to an appropriate minimization of the parasitic modes and a very weak field pattern. The peak at 146 GHz that can be observed has a significantly

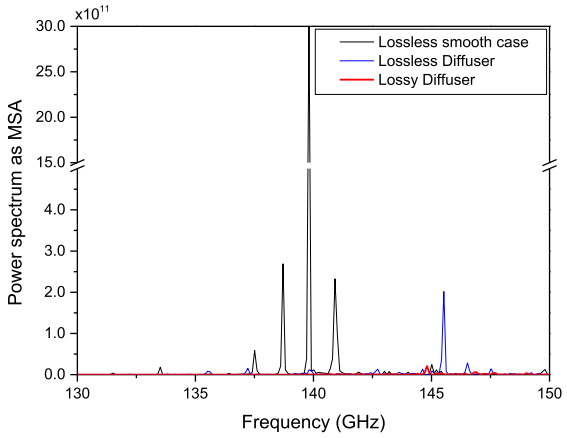


Fig. 11. Power spectrum of the electric field signal at $r = 12$ mm, $z = 40$ mm for the smooth lossless case (black line), the lossless diffuser case (blue line), and the diffuser copper case ($\sigma = 5.8 \times 10^7$ S/m) (red line).

TABLE IV
MAXIMUM OF THE POWER SPECTRUM FOR ALL MODELS

| Smooth lossless | Smooth lossy copper | Lossless with diffuser | Lossy copper with diffuser |
|---|---|---|---|
| 0 dB | -7 dB | -15.4 dB | -22 dB |

lower amplitude. This frequency probably corresponds to a frequency at which the diffusion performance of the geometry is minimal.

It should be noted that no losses were considered in this model, thus there is no Ohmic dissipation of any developed modes. To make the model more realistic, copper losses were added on the walls ($\sigma = 5.8 \times 10^7$ S/m) and the simulation was repeated. The obtained power spectrum for this case is depicted in Fig. 11 (red line). It was found that, even with the relatively low value of the losses of copper, the power spectrum was almost fully suppressed, indicating the effective suppression of all possible parasitic modes in the structure.

## IV. COMPARISON OF THE RESULTS AND DISCUSSION

In the above sections, results were presented for the following cases: smooth lossless model, smooth lossy model with copper walls ($\sigma = 5.8 \times 10^7$ S/m), smooth highly lossy model ($\sigma = 10^5$ S/m), lossless diffuser model, and lossy diffuser model with copper walls ($\sigma = 5.8 \times 10^7$ S/m). Table IV summarizes the obtained results for the maximum of the power spectrum in dB, for each of these cases (with respect to the smooth lossless model). These results show that the addition of copper losses to the smooth model suppresses the maximum of the obtained power by 80% (thus 20% still remaining), whereas in the lossless diffuser model the power reduction is 97%. In the diffuser model with copper losses, a power reduction of 99.4% is achieved. It should be noted that the remaining 0.6% is quite small, in the sense that the obtained power level is comparable to the level of the numerical noise appearing in the obtained spectrum. For this reason, such a small value could well be attributed to numerical errors.

For each case considered, we also studied the effect of the developed electric field on the beam properties. For this

TABLE V
COMPARISON OF THE BEAM PROPERTIES FOR ALL CASES

| Case | Initial $E_{kin}$ (keV) | Final $E_{kin}$ (keV) | $\Delta E_{kin}/E_{kin}$ (%) | Final $\delta\gamma$ (% rms) |
|---|---|---|---|---|
| Smooth lossless | 79.31 | 63.47 | 19.97 | 2.78 |
| Smooth lossy Cu ($\sigma = 5.8\times10^7$ S/m) | 79.31 | 75.73 | 4.51 | 2.25 |
| Smooth highly lossy ($\sigma = 10^5$ S/m) | 79.36 | 79.00 | 0.45 | 0.10 |
| Diffuser (lossless) | 79.36 | 78.29 | 1.35 | 1.21 |
| Diffuser (lossy Cu) ($\sigma = 5.8\times10^7$ S/m) | 79.36 | 78.39 | 1.22 | 0.81 |

purpose, the electron beam properties were calculated at both ends of the structure at $t = 20$ ns. In particular, a slice with thickness of 1 mm was considered at each end and of the structure and the average relativistic factor $\gamma$ value was calculated, based on the velocities of all electrons located in each slice at the considered timestep. The thickness of the slices was chosen such that it is large enough to contain an adequate number of electrons for accurate statistics and at the same time small enough for all electron in the slice to be as close to the ends as possible. This is necessary to minimize the effect of any RF interaction or of the space charge on the electron properties that could probably affect the calculated statistics. The results are summarized in Table V. It was found that the excited mode in the smooth cases causes a significant reduction of the relative beam kinetic energy $\Delta E_{kin}/E_{kin}$, also increasing the $\gamma$ spread (represented by the relative -to the mean value- standard deviation). In the case of the highly lossy smooth model, both the reduction in $\gamma$ and increase in its spread $\delta\gamma$ are minimal. Since in this case the high losses ensure no parasitic excitation, it can be deduced that the observed effect is either numerical or due to space-charge effects, which affect the beam energy due to the limited length considered in the simulations.

In the case of the models with diffusive geometry, the energy reduction and the final $\delta\gamma$ are highly reduced, however, they are still larger than the initial values. It should be kept in mind though that these results are numerical. Since, in order to calculate the beam statistics, slices with a thickness of 1 mm were considered, the calculated properties do not correspond exactly at the ends of the structure. Instead, they are affected by the space charges appearing in the structure and by its finite length, in conjunction with the applied boundary conditions. Besides, in CST Studio Suite it has been seen that both $\gamma$ and $\delta\gamma$ vary along the structure, even when no interaction takes place, because of space-charge effects. To illustrate this effect, Fig. 12 depicts the average $\gamma$ value along the $z$-axis at steady state for the smooth lossless model, when RF fields are fully ignored. It can be seen, that the average $\gamma$ value is reduced toward the middle of the structure, due to the space charge depression. This depression is approximately 2.76 kV. Fig. 13 shows the energy distribution at the entrance ($z \approx 71.8$ mm) and the exit ($z \approx 0$ mm) of the smooth lossless structure,

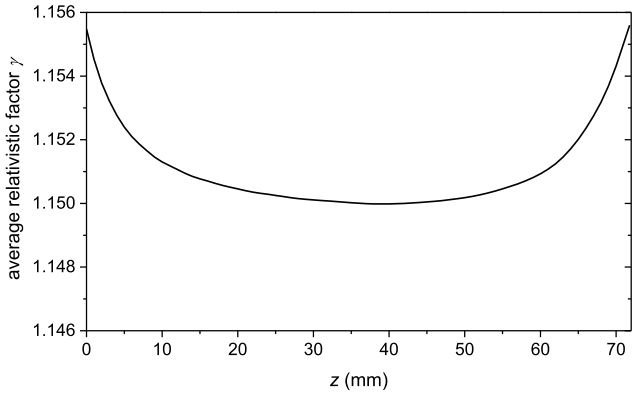


Fig. 12. Average $\gamma$ value along the $z$-axis for the smooth lossless case, when fully ignoring any RF field. The space charge depression is visible.

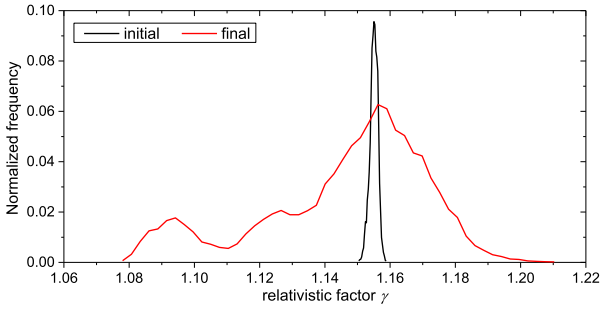


Fig. 13. Energy distribution ($\gamma$ value) of electrons at both ends of the structure (initial at $z \approx 71.8$ mm and final at $z \approx 0$ mm).

both calculated in 1 mm thick slices. It can be seen that, near the entrance, the obtained distribution is close to the imposed uniform one, whereas near the exit, the average $\gamma$ has been reduced and the energy spread has increased.

Due to the above-mentioned factors, it is expected to have reduced accuracy, however a trend between each considered case can easily be found. For this reason, the obtained beam energy spread $\delta\gamma$ may well be overestimated. This can be also seen in the case of the highly lossy smooth model, in which the gamma has changed and $\delta\gamma$ has doubled, even though no parasitic oscillation has taken place, due to the extremely high losses applied.

Of course, these results could also indicate that some weak interaction is still present in the structure. It should be noted however that the diffusive geometry used in this work was the simplest one could design and without any further optimization. Even though, the results clearly show that the concept is effective and quite promising. It is expected that by carefully optimizing the diffusive geometry and probably choosing a metal alloy with higher losses, full suppression could be achieved in a beam tunnel structure.

The importance of these findings is that the design of the diffusive geometry is simple and quite straightforward, and the use of ceramic materials is totally avoided, whereas the manufacturing process of the structure is expected to be much simpler compared to that of the existing stacked beam tunnels. Therefore, the use of this concept could reduce the manufacturing complexity and cost, whereas the obtained

results have shown a superior behavior compared to other simple solutions.

## V. Summary and Conclusion

The concept of fully metallic gyrotron beam tunnels was investigated. A smooth-wall tapered fully metallic beam tunnel structure was designed and simulated with CST Studio Suite, with and without losses and the effect of the losses on the excited mode was investigated. A simple diffusive geometry based on the Schroeder diffuser theory was designed and added to the structure. It was found that the diffuser effectively suppresses the excited fields and, when typical Ohmic losses were introduced, the parasitic modes were fully eliminated. This result is quite promising, and it is expected that a carefully optimized diffusive geometry along with a lossy metal alloy could well be used in fully metallic gyrotron beam tunnels to effectively suppress unwanted parasitic oscillations.

## References


[1] G. G. Denisov, V. E. Zapevalov, A. G. Litvak, and V. E. Myasnikov, "Megawatt gyrotrons for ECR heating and current-drive systems in controlled-fusion facilities," *Radiophys. Quantum Electron.*, vol. 46, no. 10, pp. 757–768, 2003, doi: 10.1023/B:RAQE.0000026869.75334.a1.

[2] G. S. Nusinovich, *Introduction to the Physics of Gyrotrons*. Baltimore, MD, USA: The Johns Hopkins Univ. Press, 2004.

[3] M. V. Kartikeyan, E. Borie, and M. K. A. Thumm, *Gyrotrons: High-Power Microwave and Millimeter Wave Technology*. Berlin, Germany: Springer, 2004.

[4] C. Edgecombe, *Gyrotron Oscillators*. London, U.K.: Taylor & Francis, 1993.

[5] V. Kesari and B. N. Basu, *High Power Microwave Tubes: Basics and Trends*, vol. 2. San Rafael, CA, USA: Morgan & Claypool, 2018.

[6] J. Genoud, S. Alberti, J.-P. Hogge, I. G. Tigelis, G. P. Latsas, and I. G. Chelis, "Modeling of parasitic oscillations in smooth-wall circular symmetric dielectric-loaded gyrotron beam ducts," *Phys. Plasmas*, vol. 26, no. 12, Dec. 2019, doi: 10.1063/1.5130637.

[7] G. Gantenbein et al., "Experimental investigations and analysis of parasitic RF oscillations in high-power gyrotrons," *IEEE Trans. Plasma Sci.*, vol. 38, no. 6, pp. 1168–1177, Jun. 2010, doi: 10.1109/TPS.2010.2041366.

[8] G. P. Latsas, Z. C. Ioannidis, and I. G. Tigelis, "Dependence of parasitic modes on geometry and attenuation in gyrotron beam tunnels," *IEEE Trans. Plasma Sci.*, vol. 40, no. 6, pp. 1538–1544, Jun. 2012, doi: 10.1109/TPS.2012.2192294.

[9] I. G. Chelis, D. V. Peponis, G. P. Latsas, and I. G. Tigelis, "Increasing the diffraction losses in gyrotron beam tunnels for improved suppression of parasitic oscillations," in *Proc. 44th Int. Conf. Infr., Millim., Terahertz Waves (IRMMW-THz)*, Paris, France, Sep. 2019, pp. 1–2, doi: 10.1109/IRMMW-THz.2019.8874402.

[10] K. Sakamoto et al., "Development of 170 and 110 GHz gyrotrons for fusion devices," *Nucl. Fusion*, vol. 43, no. 8, pp. 729–737, Aug. 2003, doi: 10.1088/0029-5515/43/8/314.

[11] I. I. Antakov, I. G. Gachev, and E. V. Zasypkin, "Self-excitation of spurious oscillations in the drift region of gyrotrons and their influence on gyrotron operation," *IEEE Trans. Plasma Sci.*, vol. 22, no. 5, pp. 878–882, Oct. 1994, doi: 10.1109/27.338303.

[12] Z. C. Ioannidis, I. Chelis, G. Gantenbein, T. Rzesnicki, and J. Jelonnek, "Experimental classification and enhanced suppression of parasitic oscillations in gyrotron beam tunnels," *IEEE Trans. Electron Devices*, vol. 67, no. 12, pp. 5783–5789, Dec. 2020, doi: 10.1109/TED.2020.3025751.

[13] I. G. Chelis, K. A. Avramidis, Z. C. Ioannidis, and I. G. Tigelis, "Improved suppression of parasitic oscillations in gyrotron beam tunnels by proper selection of the lossy ceramic material," *IEEE Trans. Electron Devices*, vol. 65, no. 6, pp. 2301–2307, Jun. 2018, doi: 10.1109/TED.2017.2784198.

[14] Z. C. Ioannidis et al., "Generation of 1.5 MW-140 GHz pulses with the modular pre-prototype gyrotron for W7-X," *IEEE Electron Device Lett.*, vol. 42, no. 6, pp. 939–942, Jun. 2021, doi: 10.1109/LED.2021.3073221.

[15] G. S. Nusinovich, M. K. A. Thumm, and M. I. Petelin, "The gyrotron at 50: Historical overview," *J. Infr., Millim., THz Waves*, vol. 35, no. 4, pp. 325–381, Apr. 2014, doi: 10.1007/s10762-014-0050-7.

[16] G. P. Latsas, A. I. Zisis, and I. G. Tigelis, "Computational studies on the suppression of parasitic oscillations in gyrotron beam tunnels," *IEEE Trans. Electron Devices*, vol. 65, no. 8, pp. 3479–3485, Aug. 2018, doi: 10.1109/TED.2018.2840829.

[17] T. Rzesnicki et al., "2.2-MW record power of the 170-GHz European preprototype coaxial-cavity gyrotron for ITER," *IEEE Trans. Plasma Sci.*, vol. 38, no. 6, pp. 1141–1149, Jun. 2010, doi: 10.1109/TPS.2010.2040842.

[18] A. Litvak, K. Sakamoto, and M. Thumm, "Innovation on high-power long-pulse gyrotrons," *Plasma Phys. Controlled Fusion*, vol. 53, no. 12, Dec. 2011, Art. no. 124002, doi: 10.1088/0741-3335/53/12/124002.

[19] M. Pedrozzi, S. Alberti, J. P. Hogge, M. Q. Tran, and T. M. Tran, "Electron beam instabilities in gyrotron beam tunnels," *Phys. Plasmas*, vol. 5, no. 6, pp. 2421–2430, Jun. 1998, doi: 10.1063/1.872918.

[20] Z. C. Ioannidis et al., "Recent experiments with the European 1 MW, 170 GHz industrial CW and short-pulse gyrotrons for ITER," *Fusion Eng. Des.*, vol. 146, pp. 349–352, Sep. 2019, doi: 10.1016/j.fusengdes.2018.12.065.

[21] H. P. Laqua and S. Ponomarenko, "Suppression of parasitic modes in a cylindrical gyrotron beam tunnel by a wall corrugation with Schroeder diffuser structures," *IEEE Trans. Plasma Sci*.

[22] H. P. Laqua, S. Ponomarenko, G. Gantenbein, J. Jelonnek, and T. Rzesnicki, "Breaking symmetry in gyrotrons by Schroeder diffusor structures," in *Proc. 22nd Joint Workshop Electron Cyclotron Emission (ECE) Electron Cyclotron Resonance Heating (ECRH)*, Daejeon, (South) Korea, Apr. 2024.

[23] M. R. Schroeder, "Diffuse sound reflection by maximum-length sequences," *J. Acoust. Soc. Amer.*, vol. 57, no. 1, pp. 149–150, Jan. 1975, doi: 10.1121/1.380425.

[24] M. R. Schroeder, "Binaural dissimilarity and optimum ceilings for concert halls: More lateral sound diffusion," *J. Acoust. Soc. Amer.*, vol. 65, no. 4, pp. 958–963, Apr. 1979, doi: 10.1121/1.382601.

[25] T. J. Cox and Y. W. Lam, "Prediction and evaluation of the scattering from quadratic residue diffusers," *J. Acoust. Soc. Amer.*, vol. 95, no. 1, pp. 297–305, Jan. 1994, doi: 10.1121/1.408361.

[26] T. J. Cox and P. D'Antonio, *Acoustic Absorbers and Diffusers, Theory, Design and Application*, 3rd ed. Boca Raton, FL, USA: CRC Press, 2017, doi: 10.1201/9781315369211.

[27] F. A. Everest and K. C. Pohlmann, *Master Handbook of Acoustics*, 6th ed. New York, NY, USA: McGraw-Hill, 2015.

[28] A. J. Lock, "Development of a 2D boundary element method to model Schroeder acoustic diffusers," B.Sc thesis, College Sci. Eng., Univ. Tasmania, Australia, Hobart, TAS, Australia, 2014, doi: 10.25959/23242181.v1.

[29] E. Rhee, H. Kim, and C. Park, "Advanced electromagnetic field uniformity in reverberation chamber," *Adv. Sci. Technol. Lett.*, vol. 65, pp. 65–68, Jan. 2014, doi: 10.14257/astl.2014.65.16.

[30] M. Jaax, S. Wolff, B. Laegel, and H. Fouckhardt, "Optical and THz Galois diffusers," *J. Eur. Opt. Society-Rapid Publications*, vol. 8, p. 13020, Mar. 2013, doi: 10.2971/jeos.2013.13020.

[31] *Dassault Systemes CST Studio Suite*. Accessed: Apr. 30, 2024. [Online]. Available: https://www.3ds.com/products/simulia/cst-studio-suite